


## Article

# Design of a Low-Cost and High-Precision Measurement System Suitable for Organic Transistors

Vratislav Režo \* and Martin Weis 

Faculty of Electrical Engineering and Information Technology, Slovak University of Technology in Bratislava, 841 04 Bratislava, Slovakia; martin.weis@stuba.sk

\* Correspondence: vratislav.rezo@stuba.sk

**Abstract:** Organic field-effect transistors (OFETs) require ultra-precise electrical measurements due to their unique charge transport mechanisms and sensitivity to environmental factors, yet commercial semiconductor parameter analysers capable of such measurements are prohibitively expensive for many research laboratories. This study introduces a novel, cost-effective, and portable setup for high-precision OFET characterisation that addresses this critical need, providing a feasible substitute for conventional analysers costing tens of thousands of dollars. The suggested system incorporates measurement, data processing, and graphical visualisation capabilities, together with Bluetooth connectivity for local operation and Wi-Fi functionality for remote data monitoring. The device consists of a motherboard and specialised cards for low-current measurement, voltage measurement, and voltage generation, providing comprehensive OFET characterisation, including transfer and output characteristics, in accordance with IEEE-1620 standards. The system can measure current from picoamperes to milliamperes, with voltage measurements supported by high input resistance (>100 M $\Omega$ ) and a voltage generation range of  $-30$  V to  $+30$  V. This versatile and accessible approach greatly improves the opportunities for future OFET research and development.

**Keywords:** analogue–digital converter; measurement; picoamperes; current measurement; organic transistors



**Citation:** Režo, V.; Weis, M. Design of a Low-Cost and High-Precision Measurement System Suitable for Organic Transistors. *Electronics* **2024**, *13*, 4475. <https://doi.org/10.3390/electronics13224475>

Academic Editors: Alkiviadis Hatzopoulos, Nestor Evmorfopoulos and George I. Stamoulis

Received: 9 October 2024  
Revised: 8 November 2024  
Accepted: 12 November 2024  
Published: 14 November 2024



**Copyright:** © 2024 by the authors. Licensee MDPI, Basel, Switzerland. This article is an open access article distributed under the terms and conditions of the Creative Commons Attribution (CC BY) license (<https://creativecommons.org/licenses/by/4.0/>).

## 1. Introduction

Organic electronics is an exciting new field of electronics which involves the application of molecular semiconductors in electronic devices [1]. The interest in organic electronics comes primarily from the revolutionary deposition methods that made flexible and printed electronics possible, therefore providing exceptional potential for the development of lightweight, cost-effective, and mechanically flexible devices [2,3]. This very promising technology has already achieved notable success in a wide range of applications, such as organic light-emitting diode (OLED) displays, organic solar cells, and organic field-effect transistors (OFETs) [4–7]. The unique features of organic materials, such as their tailored molecular structure for specific applications, their capacity to use solution processing, and their mechanical flexibility, have initiated new opportunities for development in consumer electronics, energy harvesting, and sensing technology.

Out of all the applications, sensors based on organic electronics have attracted significant interest as very prospective pioneers in the field of sensing technology. The envisioned applications cover a broad range, including chemical sensors with molecular recognition capabilities [8], as well as gas sensors [9] and mechanical sensors [10]. These devices have the capacity to provide extremely precise and sensitive detecting mechanisms, often imitating biological sensing systems. Nevertheless, a common difficulty encountered by such sensors is their low output signal, which may limit their practical applicability.

Within this particular framework, organic transistors have been suggested as highly appropriate options for sensing applications. A notable advantage of transistors is their

intrinsic nature, which enables the direct amplification of low sensing signals within the device [11]. The incorporation of sensing and signal amplification into a single component presents the possibility of increased sensitivity and better signal-to-noise ratios in comparison to conventional sensing methods such as resistive elements [11,12].

However, the development of sensors based on organic electronics is not free of inevitable challenges. Effective operation of these devices frequently requires large, applied voltages, therefore facing difficulties in their integration into low-power systems. Moreover, they typically demonstrate relatively low output currents, which poses a significant challenge for the detection and processing of signals [13]. Hence, there is a pressing need for the development of low-cost, highly precise measurement techniques that can detect and measure these low currents [14–16]. This will ultimately facilitate their extensive use in many domains, notably environmental monitoring and healthcare diagnostics.

The precise measurement of low currents, particularly in the range of nanoamperes to femtoamperes, represents a critical challenge in organic electronics research and development. While commercial semiconductor parameter analysers offer the required measurement precision, their high cost (typically exceeding USD 50,000) and bulky nature significantly limit widespread access, especially in academic research laboratories and small-scale development facilities. This creates a substantial barrier to entry for many researchers for the rapid advancement of organic electronics technology. In other words, even though organic electronic devices have low-cost fabrication, the costly characterisation techniques suppress the development of this field. Moreover, existing low-cost measurement solutions often fail to provide the necessary measurement precision, automation capabilities, and compliance with standardised measurement protocols required for reliable OFET characterisation. This gap between high-end commercial systems and accessible measurement solutions has become a bottleneck in the development and optimisation of organic electronic devices, particularly in sensing applications where precise current measurements are crucial. Therefore, there is an urgent need for innovative measurement systems that can combine high precision, automation capabilities, and cost-effectiveness while maintaining compliance with established measurement standards such as IEEE-1620. Such systems would significantly accelerate research progress in organic electronics and facilitate their transition from laboratory demonstrations to practical applications.

An effective approach for quantifying low currents is to use a shunt resistor [17]. This technique involves placing a precisely determined resistor in series with the current flow and thereafter determining the voltage drop across the resistance. Although this technique is reasonably straightforward and cost-effective, it can lead to significant loading effects and is constrained by the thermal noise of the resistor, particularly when handling very low currents.

To minimise the loading effects caused by the simple shunt resistors, it is possible to incorporate a buffer amplifier. This arrangement, referred to as a shunt resistor with a buffer amplifier, ensures a high input impedance for current sensing while providing a low-impedance voltage output. The amplifier buffer separates the measuring circuit from the following stages, thereby minimising the errors caused by loading.

The Rogowski coil provides an interesting solution for applications that require non-invasive current measurements, especially in power systems and high-frequency circuits [18]. When situated around a conductor, an air-core toroidal coil generates an output voltage that is directly proportional to the rate of change of the current. Although highly effective in measuring alternating currents and transients, this approach requires integration of the output signal and is less appropriate for accurate direct current measurements. Furthermore, it is less sensitive in the case of low-current measurements.

The operational transconductance amplifier (OTA) directly transforms the input current into an output current. This technique can offer high bandwidth and low noise, making it suitable for a wide range of current measurement applications [19–21]. Nevertheless, the linearity and dynamic range of OTAs can be limiting factors in high-precision measurements; hence, several approaches have been suggested to mitigate these limitations.

Amplifier-based approaches that exploit either resistive or capacitive feedback are adaptable and extensively employed for low-current measurements. The resistive feedback arrangement, that is, a transimpedance amplifier, converts the input current to a voltage by passing it through a high-value feedback resistor. This technique provides exceptional linearity and a broad dynamic range, although its performance may be constrained by thermal noise generated by the feedback resistor when conducting very low currents. The capacitive feedback technique, alternatively referred to as the integrating current amplifier, employs a capacitor in the feedback loop, as opposed to a resistor. The integration of the input current over time in this design resulted in the generation of a rising output voltage. Despite its ability to achieve extremely low noise levels and reduced susceptibility to parasitic capacitances, this approach requires regular reset mechanisms to avoid saturation.

Various methods for low-current measurements exhibit distinct compromises in terms of sensitivity, bandwidth, noise level, and complexity. Therefore, the selection of the appropriate technique is significantly influenced by the particular demands of the application, such as the expected current range, preferred measurement speed, and limitations in system integration. A detailed comparison is described in Supplementary Information.

This study offers three significant contributions to address the issues in OFET characterisation. We present an innovative measuring system design that attains high-precision measurements in comparison with commercial semiconductor parameter analysers at approximately one-tenth of the expense. Second, we created specialised measuring cards designed to accommodate the distinct electrical properties of OFETs, facilitating current measurements ranging from nanoamperes to microamperes and voltage excitations of up to  $\pm 30$  V, with the measurement precision corroborated by industry-standard equipment. We employed an automated measurement algorithm that follows IEEE-1620 standards [22], facilitating systematic device characterisation and data analysis via an integrated software interface. The proposed system matches the measuring capabilities of standard parametric analysers while providing superior portability and connectivity and managing it appropriately for in situ characterisation and remote monitoring applications. This comprehensive solution signifies a substantial advancement in democratising OFET research and development by offering an accessible yet robust alternative to expensive commercial systems.

## 2. The Design and Development of an Organic Transistor Measurement System

Before the beginning of the design measurement system, we had to determine the voltage and current ranges of organic transistors of widely used organic semiconductors, namely pentacene and dinaphtho [2,3-b:2',3'-f] thieno [3,2-b] thiophene (DNTT), which can be used as a reliable reference. The fabrication procedure of OFET devices used here was described previously [23]. As illustrated in Figure 1, transfer characteristics indicate the need to set the minimum current sensing limit to 1 pA and the maximum current limit up to 20 mA, with the voltage bias in the range of  $\pm 30$  V. It should be noted that even though the highest output current of the investigated device reaches 120  $\mu$ A, devices with short channel lengths may exhibit maximum output currents as high as several milliamps.

Therefore, the first step in creating such a complex and sophisticated measurement system was to divide it into functional blocks, as shown in Figure 2. Each functional block has its own role, whether it is a voltage measurement block, a small-current measurement block with a large dynamic range, or a voltage generation block. We then described these functional blocks with their basic characteristics and began to create initial schematics and simulations for them.

We decided to use an operational amplifier in a non-inverting configuration instead of a JFET voltage follower for voltage measurement. This was due to the temperature stability of the measurement, noise immunity, and electrostatic immunity. For the current measurement, we chose to use a transimpedance amplifier that creates a virtual ground and accurately converts current to voltage. In addition, we decided on a simple operational amplifier circuit with a fixed gain for voltage generation.

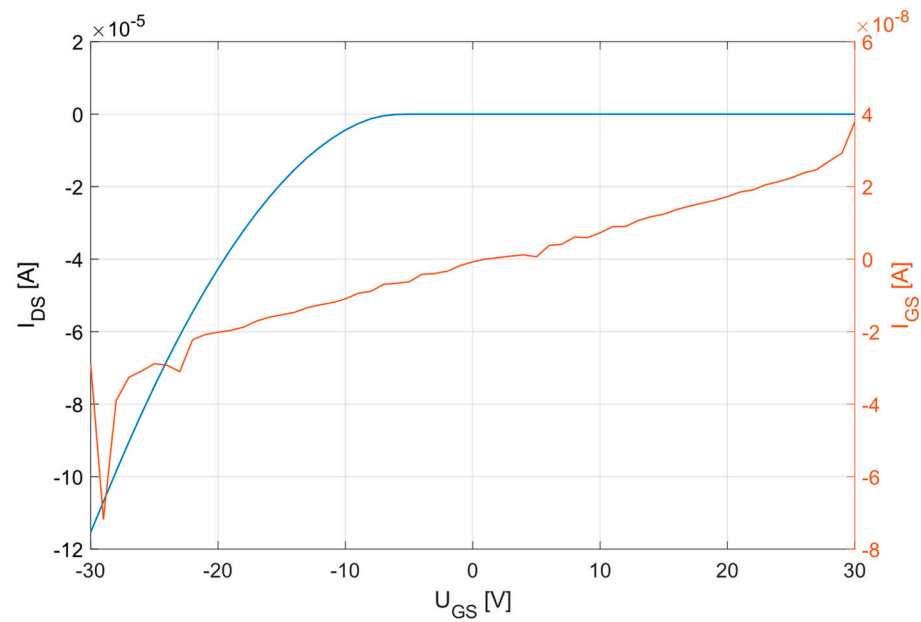


**Figure 1.** Reference measurement of OFET with top-contact bottom-gate topology based on DNNT organic semiconductor and with 2.5 mm wide channel and 125  $\mu$ m long channel.

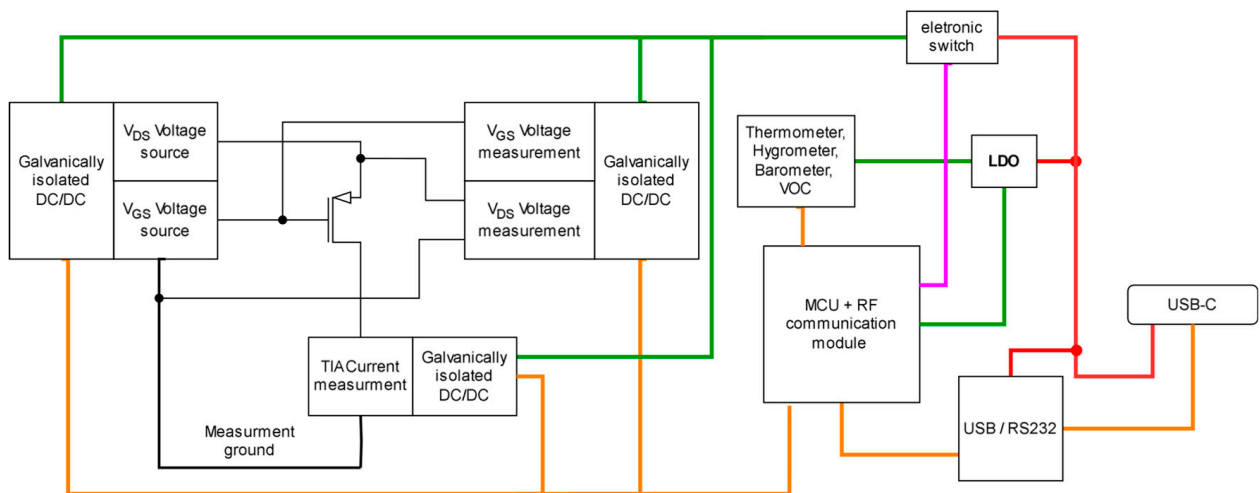


**Figure 2.** Block diagram for the whole measurement system. Orange represents the communication lines, while red and green are primary voltage and stabilised voltage biases, respectively. The purple line stands for the voltage turn-on signal.

After the initial schematics and simulations, we determined the critical parameters for the components used in each module and searched for the most optimal components on the market that would be suitable for the measurement system. The critical parameters for the operational amplifier in the current measurement block were input resistance, input leakage current, and inherent noise. The critical parameters for the passive components involved in the current-to-voltage conversion were manufacturing accuracy, package, and material. Similarly, we identified the parameters for the voltage measurement block, where the operational amplifier also had to have high input resistance and low input leakage currents, while the amplifiers had to operate with voltages as high as  $\pm 30$  V. Similarly, the operational amplifier in the voltage generation block had to work with these voltages and provide sufficient output currents of up to 20 mA.

After determining the critical parameters, we selected the LMP7721 operational amplifier for the voltage measurement block, which has an input leakage current of only 3 fA and

a noise level of only  $0.01 \text{ pA}/\sqrt{\text{Hz}}$ . For the resistors for current-to-voltage conversion, we chose thin-film metal SMD resistors in the SMD2512 package. We also chose COG capacitors for filtering and stabilisation due to the frequency properties of the material itself.

When choosing an operational amplifier for voltage measurement, we came across the LTC6090 operational amplifier, which met the criteria for the power amplifier of the voltage generation block with its parameters, as shown in Figure 3. The details of the LMP7721 and LTC6090 comparison are described in Supplementary Information.

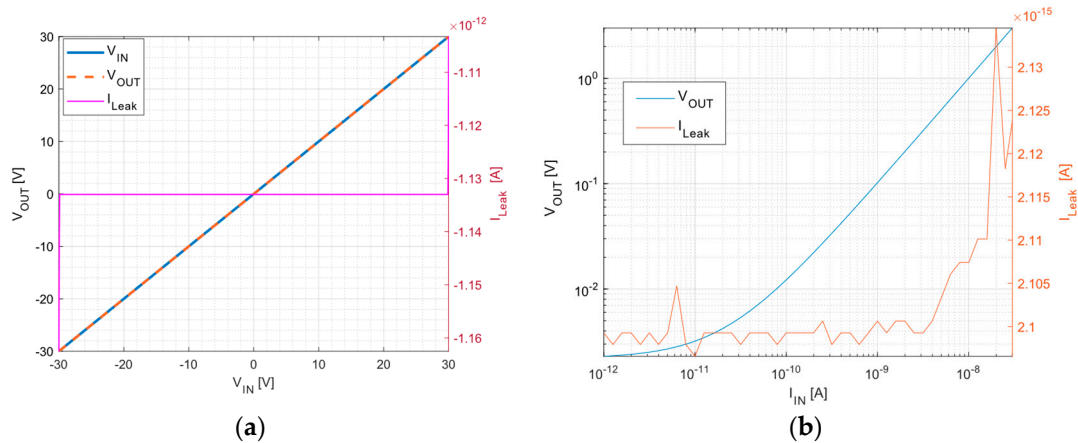


**Figure 3.** Simulation of (a) voltage follower with LTC6090 and (b) transimpedance amplifier with LMP7721.

For the digitisation of the measured data, we decided to use the MCP3562T ADC converter, which emerged victorious from the comparison due to its resolution, linearity of conversion, speed, and low noise. For the generation of the voltage signal, we used DAC8562, which came out on top in the comparison due to its resolution, linearity of conversion, and output noise.

After selecting these components, we went through the simulations again to verify functionality and adjust the values of the passive components. After the simulations, we moved on to the PCB design, where we had to use special PCB-shaping techniques from the IPC-2221 standard [24] for several modules to achieve the lowest possible leakage currents and the best signal integrity. The details on PCB shaping are depicted in Supplementary Information. Then, after the design, these modules were manufactured and assembled. This resulted in three types of cards: a current measurement card, a voltage measurement card, and a voltage generation card, as illustrated in Figure 4. The use of galvanic separators to power individual modules was necessary to eliminate ground loops and suppress interference between individual cards. The details of galvanic separators are described in Supplementary Information.

Power management represents a crucial aspect of portable measurement systems, particularly for those requiring high-precision and low-noise characteristics. The presented system employs a DC power supply in the form of a powerbank, which serves dual purposes: ensuring operational autonomy and, more importantly, enhancing measurement accuracy. While portable measurement devices commonly face challenges related to power efficiency and energy storage optimisation [25–28], our primary motivation for implementing battery-based power delivery stems from the necessity to minimise measurement noise. The isolation from AC power lines significantly reduces common-mode interference and power line noise, which is particularly critical when measuring currents in the picoampere range. This approach provides stable voltage biasing and substantially improves the signal-to-noise ratio compared to AC-powered alternatives, albeit at the cost of limited operational duration. The trade-off between measurement precision and power autonomy was carefully considered, with priority given to measurement integrity given the specialised requirements of OFET characterisation.

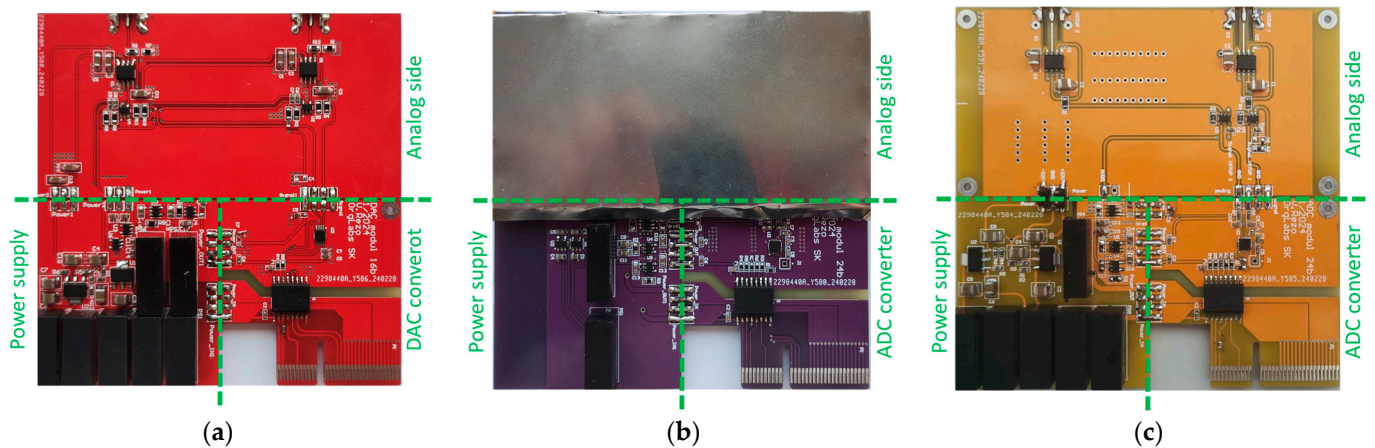


**Figure 4.** Assembled cards: (a) card for generating voltage, (b) card for measuring small current with proper shielding, and (c) card for measuring voltage.

### 3. Calibration of Measurement System

Calibration and confirmation of suitability and functionality of the current measurement card for each range were performed with a sourcemetre, Keithley 2400 (Keithley Instruments, Solon, OH, USA), and then verified with a semiconductor parameter analyser, Keysight B1500A (Keysight Technologies, Santa Rosa, CA, USA). The measurement of the measurement card is depicted in Figure 5a.

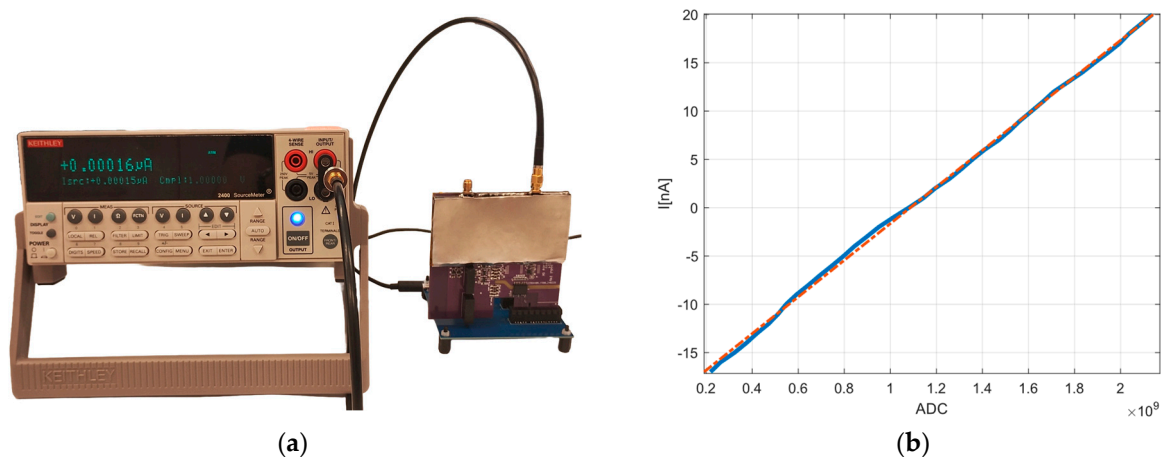


**Figure 5.** (a) Setup of calibration of a current measurement card with KEITHLEY 2400 and (b) the calibration curve for the lowest current range  $\pm 20$  nA.

After measuring all the calibration curves, we proceeded to their linear interpolation due to the shape of the curve, as shown in Figure 5b. After interpolating the lines for all current ranges, we extracted the values of the calibration coefficients in Table 1. After subsequent comparison of these current measurement errors against the Keysight 2400 calibrator, we found that in the middle range, the error of our metre is 0.7173%, which is several times larger against Keysight's 0.033% + 2 nA over the  $\pm 10$   $\mu$ A range. For the largest range, the error is 0.012%, which is 3.75 times better than Keysight 2400, where the error is 0.045% + 2  $\mu$ A.

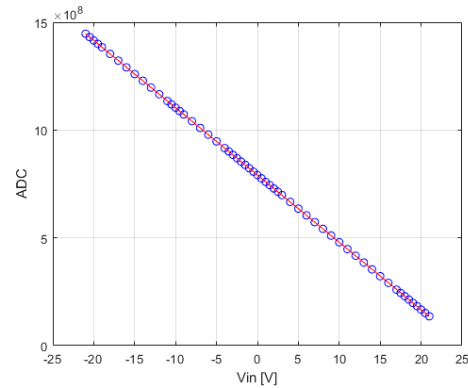
Once we calibrated the current measurement card, we proceeded to calibrate the voltage measurement card, which we also performed with Keithley 2400 and then verified the results with Keysight B1500A. The measurement of the measurement card is shown in Figure 6a.

**Table 1.** Calibration table for current measure card. The slope  $k$  and current offset and  $q$  characterise the linear function, while  $R^2$  stands for the coefficient of determination.

Range	$k$ [A/ADC]	$q$ [A]	$R^2$
Low	$1.895597706071 \times 10^{-17}$	$-2.05947536042 \times 10^{-8}$	0.9991398002192
Medium	$2.144024559051 \times 10^{-14}$	$-2.24670935089 \times 10^{-5}$	0.999409795284554
High	$1.511222904191 \times 10^{-11}$	$-0.01644864053275$	0.999999238962402



(a)



(b)

**Figure 6.** (a) Setup of calibration of a voltage measurement card with KEITHLEY 2400 and (b) the calibration curve.

After measuring the calibration curves for channels “A” and “B”, we proceeded to interpolate them linearly due to the shape of the curve as shown in Figure 6b, which showed a linear dependence of the measured voltage versus the ADC value of the transducer. After interpolating the lines, we extracted the calibration and error coefficients for both measurement channels in Table 2, where the measurement error for channel A is 0.009911%, and for channel B, it is 0.011817%, which is comparable to the measurement error of the Keysight 2400 calibrator which is 0.02% + 2.4 mV at a voltage range of ±20 V. The measurement error of Keysight 2400 is 0.02% + 2.4 mV.

**Table 2.** Calibration table for voltage measure card. The slope  $k$  and current offset and  $q$  characterise the linear function, while  $R^2$  stands for the coefficient of determination.

Chanel	$k$ [V/ADC]	$q$ [V]	$R^2$
A	$-3.203342051835 \times 10^{-8}$	32.3468146297232	0.9999994493
B	$-3.192996937026 \times 10^{-8}$	32.2817733274844	0.9999992180

The last card that was calibrated was the voltage generation card. After measuring the calibration curves of channels “A” and “B”, linear interpolation was also used due to the shape of the curve as shown in Figure 7b, which showed a linear dependence of the generated voltage versus the DAC value of the converter. After interpolating the lines, we plotted the coefficients for the two generating channels in Table 3.

**Table 3.** Calibration table for voltage generation card. The slope  $k$  and current offset and  $q$  characterise the linear function, while  $R^2$  stands for the coefficient of determination.

Chanel	$k$ [V/DAC]	$q$ [V]	$R^2$
A	$-0.00206567442239$	33.49055542177	0.9999694520
B	$-0.00204386709738$	33.49055542177	0.9999671202

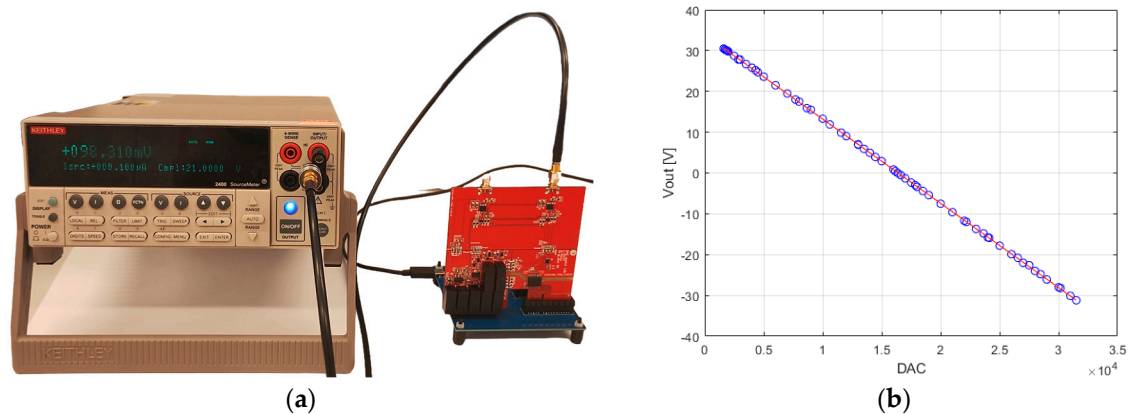


**Figure 7.** (a) Setup of calibration of a voltage generation card with KEITHLEY 2400 and (b) a calibration curve.

#### 4. Firmware

The firmware implemented appropriate filters for each measurement card after the calibration measurements. Specifically, it applied a median filter for current measurements and an Infinite Impulse Response (IIR) notch filter at 50 Hz for voltage measurements. The IIR filter coefficients were determined using the “Filter Designer” tool in Matlab. After filtering, the ADC and DAC values were converted to voltage and current values using the corresponding calibration curves.

After applying these filters and calibration curves to the firmware, a routine to self-test the measurement system was developed. Next, an algorithm was developed to measure the transistor’s transient and output characteristics. The inputs to these algorithms were voltage measurement ranges and a number of steps in measurement. Details on measurement flowcharts are shown in Supplementary Information.

The firmware measured 15 samples of voltages  $U_{GS}$  and  $U_{DS}$ , which were filtered using the IIR notch filter at 50 Hz. For current measurements, 15 samples were taken at a sampling frequency of 1 kHz, where white noise was suppressed using a median filter. The firmware then transmitted the measured data and increased the voltage  $U_{DS}$  or  $U_{GS}$ , depending on the selected measurement, by a linear step within the defined measurement limits. The algorithm also checked the specified measurement ranges to prevent setting invalid ranges that the device could not measure. To comply with the IEEE 1620 standard, a minimum of 25 measurement points was ensured for execution. The details on firmware including the pseudocode are described in Supplementary Information.

#### 5. Software for Evaluation of Organic Transistor Parameter

A critical aspect of the system is the automated evaluation of organic transistors in MATLAB R2023b, focusing specifically on the transfer characteristics of the transistor, which is shown in Figure 8. This evaluation follows the IEEE-1620 standard for identifying key parameters and involves displaying and interpreting the main features of the transfer characteristics [29].

The first parameter to determine is the threshold voltage ( $V_{th}$ ). This parameter is derived from the transfer characteristic, identifying the most stable slope within the saturation and linear regions. The slope is then extrapolated to zero current, and the intersection with the  $x$ -axis indicates the value of the linear threshold voltage. The transfer characteristic can also be used to determine the transconductance ( $G_m$ ). This parameter utilises the region with the steepest slope, and its output is expressed in Siemens (S).

To determine the saturated threshold voltage, the square root of the drain–source current ( $I_{DS}$ ) is calculated, and the most stable slope in the saturation region is marked. This slope is extrapolated to zero, where the saturated threshold voltage value is found at the zero intersection point of the extrapolated line.



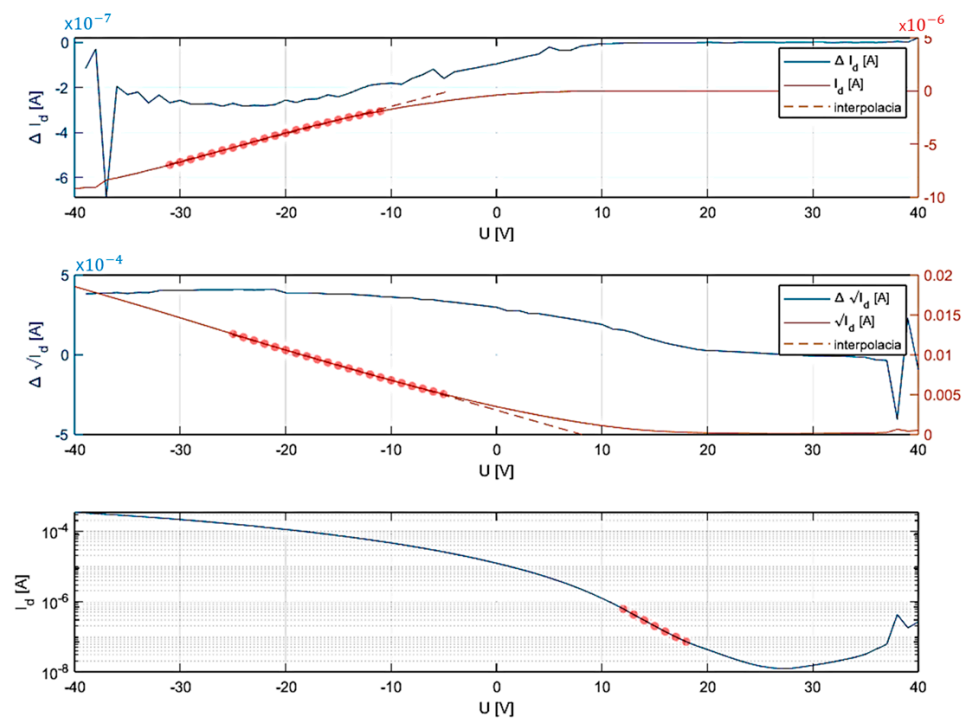


**Figure 8.** Software for evaluation of OFET parameters from the transfer characteristic. The red lines represent the linear fit to evaluate specific device parameters.

The final parameter is the subthreshold slope ( $S$ ), determined from the transfer characteristic where the current  $I_{DS}$  is in a logarithmic scale. The subthreshold slope is identified in the region with the steepest slope, where the current exhibits the greatest dynamic change relative to voltage. The output unit for this parameter is volts per decade.

## 6. Measurement Results

After debugging the firmware and software, we set about measuring using the metering system we designed. First, we verified the functionality of the measured OFET elements based on DNTT using Keysight B1500A as a reference. Subsequently, measurements were performed using our measurement instrument.

### *DNTT Organic Transistor Measurement*

The measurements themselves were performed in the dark, in a mild vacuum ( $<10^{-2}$  Pa), and at room temperature of 300 K as specified by the IEEE-1620 standard [22]. These measurements were taken on 200  $\mu\text{m}$  long and 2.5 mm wide channel transistors at a  $U_{DS}$  voltage of  $-30$  V with a  $U_{GS}$  voltage sweep from  $-30$  V to  $+30$  V. The same parameters for measuring the transmission characteristic were set on our measurement system, and Keysight B1500A with its result is shown in Figure 9b. From the translation of the measured characteristics, we can determine that the measurement system is working properly. And the maximum error was at the level of 1.72%. Table 4 summarises the main transistor parameters evaluated using the reference measurement system (Keysight B1500A) and proposed small-current measurement system. Obviously, the difference in the parameters' values is insignificant since it is lower than the estimation error or reproducibility error (in the case of effective charge carrier mobility). It should be noted here that the measurement system and the device design, see Figure 10, are protected by utility patents and designs [30–32].

The comparison of the proposed low-current measurement system with commercially available measurement systems is summarised in Tables 5 and 6.

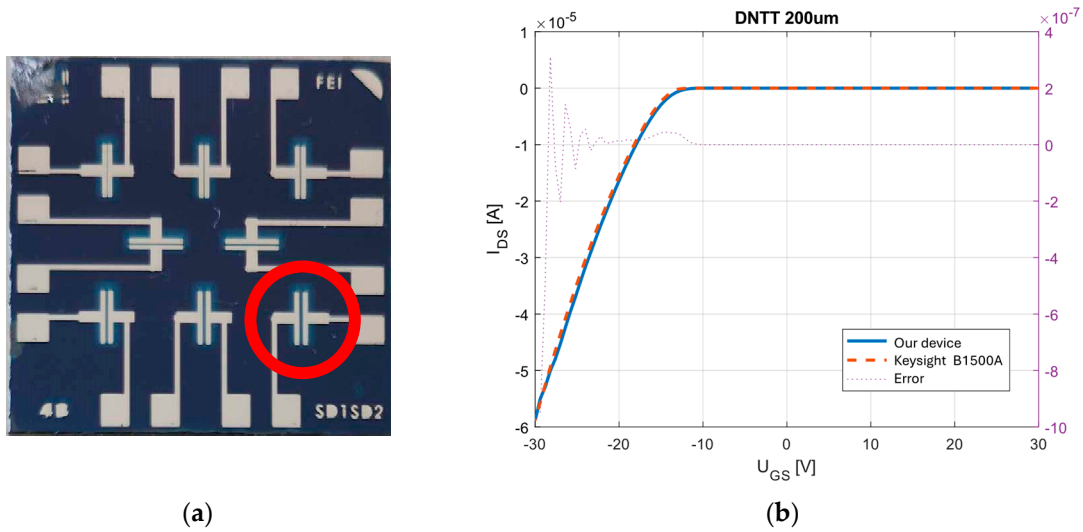


**Figure 9.** (a) Sample of DNTT transistors where the red circle points out investigated OFET device. (b) Transfer characteristics of DNTT OFET with 200  $\mu\text{m}$  channel length and 2 mm channel width.

**Table 4.** Comparison of transistor parameters evaluated using measurements performed by the Keysight B1500A system and our device. Threshold voltages ( $V_{TH}$ ) and effective charge carrier mobilities ( $\mu$ ) have been evaluated in linear and saturation regions, while the subthreshold swing ( $S_s$ ) was evaluated from the subthreshold region.

Parameters	Keysight B1500A	R <sup>2</sup>	Our Device	R <sup>2</sup>
$V_{TH,lin}$ [V]	$-17.9701 \pm 0.0624$	0.99889	$-17.0106 \pm 0.0398$	0.99934
$V_{TH,sat}$ [V]	$-11.3434 \pm 0.1711$	0.99611	$-11.2624 \pm 0.0926$	0.99824
$S_s$ [V/dec]	$0.5947 \pm 0.096$	0.99884	$0.8596 \pm 0.1387$	0.99882
$\mu_{lin}$ [ $\text{cm}^2/\text{V}\cdot\text{s}$ ]	$0.8397 \pm 0.0139$		$0.7559 \pm 0.0031$	
$\mu_{Sat}$ [ $\text{cm}^2/\text{V}\cdot\text{s}$ ]	$0.0116 \pm 4.5940 \times 10^{-6}$		$0.0114 \pm 3.0962 \times 10^{-7}$	



**Figure 10.** Design of the small-current measurement system casing. The evaluated OFET device is connected via the spring probes.

**Table 5.** Quantitative comparison of performance metrics and prices between the proposed measurement system and available commercial products.

Device	Voltage		Current			
	Range	Error	Range	Error	Range	Error
Proposed device	±30 V	0.00991%	±20 mA	0.012%	±20 nA	0.37%
Rigol DM3058E (RIGOL Technologies, Beijing, China)	±20 V	0.015% + 80 mV	±20 mA	0.095% + 4 µA	±200 µA	0.055% + 10 nA
Keithley 2400 (Keithley Instruments, Solon, OH, USA)	±20 V	0.02% + 2.4 mV	±10 mA	0.045% + 2 µA	±1 µA	0.035% + 600 pA
Keysight B1500A (Keysight Technologies, Santa Rosa, CA, USA)	±20 V	0.009% + 0.9 mV	±10 mA	0.03% + 0.2 µA	±10 nA	0.1% + 1 pA
Rigol DM858 (RIGOL Technologies, Beijing, China)	±10 V	0.03% + 40 mV	±10 mA	0.095% + 2 µA	±100 µA	0.055% + 5 nA

**Table 6.** Quantitative comparison of the proposed method with available commercial products in terms of sensitivity, bandwidth, and noise level.

Device	Voltage			Current		
	Sensitivity	Bandwidth	Noise	Sensitivity	Bandwidth	Noise
Proposed device	0.32 µV	50 kHz	−73.74 dB	18.9 fA	50 kHz	−77.13 dB
Rigol DM3058E	2 µV	20–100 kHz	−60 dB	2 nA	20–100 kHz	−60 dB
Keithley 2400	1 µV	X	−80 dB	10 pA	X	−80 dB
Keysight B1500A	2 µV	X	−90 dB	10 fA	X	−90 dB
Rigol DM858	2 µV	80 Hz	−60 dB	2 nA	80 Hz	−60 dB
GWINSTEK GPM-8310 (Good Will Instrument Co., New Taipei City, Taiwan)	2 µV	0.1–100 kHz	X	10 µA	0.1–100 kHz	X

## 7. Conclusions

This study successfully demonstrated the development of an innovative, portable, and low-cost approach for the high-precision characterisation of OFETs. The suggested device presents a viable alternative to costly semiconductor parameter analysers, possibly democratising OFET research and development in both academic and industrial environments.

We designed a modular system with interchangeable cards for current measurements, voltage measurements, and voltage generation, thus enabling flexibility and precise calibration. The firmware was developed to ensure device functionality and readiness through self-testing, whereas the control software facilitated communication via Bluetooth, allowing for accurate evaluation of transistor parameters.

Looking ahead, this research opens up several promising routes for future OFET investigation. Integrating environmental control mechanisms (e.g., temperature and humidity) into the measurement system could provide more comprehensive characterisation under different operating conditions, which is essential for practical OFET applications. Furthermore, integrating machine learning algorithms into data processing might allow for real-time analysis and prediction of OFET performance, hence expediting the optimisation process in device fabrication and design. Future development of interfaces between the measuring system and OFET fabrication equipment could enable in-line quality control and process optimisation, bridging the gap between research and manufacturing.

In conclusion, this study demonstrates a significant improvement in the accessibility and comprehensiveness of OFET characterisation. The proposed system's adaptability, portability, and economic efficiency render it an important tool for the further development of OFET technology. As organic electronics advance, measurement methods such as that shown will be essential in stimulating innovation, spanning from fundamental research to practical applications in flexible electronics, sensors, and beyond.

**Supplementary Materials:** The following supporting information can be downloaded at: <https://www.mdpi.com/article/10.3390/electronics13224475/s1>, Table S1: Comparison of various previously reported approaches; Figure S1. S2 LMP7721 and LTC6090 comparison; Figure S2. S3 LTSpice model scheme and simulation results; Figure S3. S4 PCB shaping technique; Figure S4. S6 Measurement flowcharts.

**Author Contributions:** Conceptualisation, V.R. and M.W.; methodology, V.R.; formal analysis, V.R.; writing—original draft preparation, V.R. and M.W.; funding acquisition, M.W. All authors have read and agreed to the published version of the manuscript.

**Funding:** This work was supported by the Slovak Research and Development Agency of the Ministry of Education, Science Research, and Sport of the Slovak Republic (grant numbers APVV-20-0564, APVV-20-0310, and APVV-23-0529), the Ministry of Education, Science, Research, and Sport of the Slovak Republic grant (VEGA 1/0623/23), and matching grants to resources obtained within the programme Horizon 2020 and Horizon Europe (grant number 0 01-03-V04-00028).

**Data Availability Statement:** Data will be made available upon request.

**Conflicts of Interest:** The authors declare no conflicts of interest.

## References

1. Forrest, S.R. *Organic Electronics: Foundations to Applications*; Oxford University Press: Oxford, UK, 2020.
2. Wiklund, J.; Karakoç, A.; Palko, T.; Yiğitler, H.; Ruttik, K.; Jäntti, R.; Paltakari, J. A review on printed electronics: Fabrication methods, inks, substrates, applications and environmental impacts. *J. Manuf. Mater.* **2021**, *5*, 89. [[CrossRef](#)]
3. Gao, W.; Ota, H.; Kiriya, D.; Takei, K.; Javey, A. Flexible electronics toward wearable sensing. *Acc. Chem. Res.* **2019**, *52*, 523–533. [[CrossRef](#)] [[PubMed](#)]
4. Bauri, J.; Choudhary, R.B.; Mandal, G. Recent advances in efficient emissive materials-based OLED applications: A review. *J. Mater. Sci.* **2021**, *56*, 18837–18866. [[CrossRef](#)]
5. Zhang, G.; Lin, F.R.; Qi, F.; Heumüller, T.; Distler, A.; Egelhaaf, H.J.; Li, N.; Chow, P.C.; Brabec, C.J.; Jen, A.K.Y.; et al. Renewed prospects for organic photovoltaics. *Chem. Rev.* **2022**, *122*, 14180–14274. [[CrossRef](#)]
6. Song, J.; Liu, H.; Zhao, Z.; Lin, P.; Yan, F. Flexible organic transistors for biosensing: Devices and applications. *Adv. Mater.* **2024**, *36*, 2300034. [[CrossRef](#)]
7. Lai, S.; Barbaro, M.; Bonfiglio, A. Tailoring the sensing performances of an OFET-based biosensor. *Sens. Actuator B Chem.* **2016**, *233*, 314–319. [[CrossRef](#)]
8. Demelas, M.; Lai, S.; Casula, G.; Scavetta, E.; Barbaro, M.; Bonfiglio, A. An organic, charge-modulated field effect transistor for DNA detection. *Sens. Actuator B Chem.* **2012**, *171*, 198–203. [[CrossRef](#)]
9. Zhang, C.; Chen, P.; Hu, W. Organic field-effect transistor-based gas sensors. *Chem. Soc. Rev.* **2015**, *44*, 2087–2107. [[CrossRef](#)]
10. Lamport, Z.A.; Cavallari, M.R.; Kam, K.A.; McGinn, C.K.; Yu, C.; Kymissis, I. Organic thin film transistors in mechanical sensors. *Adv. Funct. Mater.* **2020**, *30*, 2004700. [[CrossRef](#)]
11. Macchia, E.; Picca, R.A.; Manoli, K.; Di Franco, C.; Blasi, D.; Sarcina, L.; Ditaranto, N.; Cioffi, N.; Österbacka, R.; Scamarcio, G.; et al. About the amplification factors in organic bioelectronic sensors. *Mater. Horiz.* **2020**, *7*, 999–1013. [[CrossRef](#)]
12. Wang, J.; Ye, D.; Meng, Q.; Di, C.A.; Zhu, D. Advances in Organic Transistor-Based Biosensors. *Adv. Mater. Technol.* **2020**, *5*, 2000218. [[CrossRef](#)]
13. Lamport, Z.A.; Haneef, H.F.; Anand, S.; Waldrip, M.; Jurchescu, O.D. Tutorial: Organic field-effect transistors: Materials, structure and operation. *J. Appl. Phys.* **2018**, *124*, 071101. [[CrossRef](#)]
14. Taheri, H.E.; Ocheje, M.U.; St. Onge, P.B.J.; Rondeau-Gagné, S.; Mirhassani, M. Computational design of an integrated CMOS readout circuit for sensing with organic field-effect transistors. *Front. Electron.* **2021**, *2*, 725008. [[CrossRef](#)]
15. Frick, V.; Lévêque, P.; Soysal, U.; Heiser, T. Integrated high-voltage CMOS mixed-signal instrumentation system for OFET-based gas sensor. In Proceedings of the 2016 IEEE International Conference on Electronics, Circuits and Systems (ICECS), Monte Carlo, Monaco, 11–14 December 2016; IEEE: Piscataway, NJ, USA, 2016; pp. 309–312. [[CrossRef](#)]
16. Anisimov, D.S.; Chekusova, V.P.; Trul, A.A.; Abramov, A.A.; Borshchev, O.V.; Agina, E.V.; Ponomarenko, S.A. Fully integrated ultra-sensitive electronic nose based on organic field-effect transistors. *Sci. Rep.* **2021**, *11*, 10683. [[CrossRef](#)] [[PubMed](#)]
17. Iwansson, K.; Sinapius, G.; Hoornaert, W.; Middelhoek, S. *Measuring Current Voltage and Power Handbook of Sensors and Actuators*; Elsevier: Amsterdam, The Netherlands, 1999; Volume 7.
18. Jiao, C.; Zhang, J.; Zhao, Z.; Zhang, Z.; Fan, Y. Research on small square PCB Rogowski coil measuring transient current in the power electronics devices. *Sensors* **2019**, *19*, 4176. [[CrossRef](#)]
19. Ferrari, G.; Gozzini, F.; Molari, A.; Sampietro, M. Transimpedance amplifier for high sensitivity current measurements on nanodevices. *IEEE J. Solid-State Circuits* **2009**, *44*, 1609–1616. [[CrossRef](#)]
20. Rajabzadeh, M.; Djekic, D.; Haerberle, M.; Becker, J.; Anders, J.; Ortmanns, M. Comparison study of integrated potentiostats: Resistive-TIA, capacitive-TIA, CT  $\Sigma\Delta$  modulator. In Proceedings of the 2018 IEEE International Symposium on Circuits and Systems (ISCAS), Florence, Italy, 27–30 May 2018; IEEE: Piscataway, NJ, USA, 2018; pp. 1–5. [[CrossRef](#)]

21. Goldstein, B.; Kim, D.; Xu, J.; Vanderlick, T.K.; Culurciello, E. CMOS low current measurement system for biomedical applications. *IEEE Trans. Biomed. Circuits Syst.* **2012**, *6*, 111–119. [[CrossRef](#)]
22. *IEEE 1620-2008*; Standard for Test Methods for the Characterization of Organic Transistors and Materials. IEEE: Piscataway, NJ, USA, 2008. Available online: <https://standards.ieee.org/ieee/1620/3981/> (accessed on 8 October 2024).
23. Hanic, M.; Vincze, T.; Rezo, V.; Weis, M. Nature of Ohmic and Schottky contacts on pentacene-based organic field-effect transistor. *Synth. Met.* **2024**, *305*, 117590. [[CrossRef](#)]
24. *IPC-2221*; Revision C—Standard Only: Generic Standard on Printed Board Design. IPC: Bannockburn, IL, USA, 2023. Available online: <https://shop.ipc.org/ipc-2221/ipc-2221-standard-only/Revision-c/english> (accessed on 8 October 2024).
25. Amir, M.; Deshmukh, R.G.; Khalid, H.M.; Said, Z.; Raza, A.; Muyeen, S.M.; Nizami, A.S.; Elavarasan, R.M.; Saidur, R.; Sopian, K. Energy storage technologies: An integrated survey of developments, global economical/environmental effects, optimal scheduling model, and sustainable adaption policies. *J. Energy Storage* **2023**, *72*, 108694. [[CrossRef](#)]
26. Russ, B.; Glauddell, A.; Urban, J.J.; Chabinyk, M.L.; Segalman, R.A. Organic thermoelectric materials for energy harvesting and temperature control. *Nat. Rev. Mater.* **2016**, *1*, 16050. [[CrossRef](#)]
27. ur Rehman, A.; Alblushi, I.G.; Zia, M.F.; Khalid, H.M.; Inayat, U.; Benbouzid, M.; Muyeen, S.M.; Hussain, G.A. A solar-powered multi-functional portable charging device (SPMFPCD) with internet-of-things (IoT)-based real-time monitoring—An innovative scheme towards energy access and management. *Green Technol. Sustain.* **2025**, *3*, 100134. [[CrossRef](#)]
28. Elahi, H.; Munir, K.; Eugeni, M.; Atek, S.; Gaudenzi, P. Energy harvesting towards self-powered IoT devices. *Energies* **2020**, *13*, 5528. [[CrossRef](#)]
29. *IEEE 1620-2004*; Standard for Test Methods for the Characterization of Organic Transistors and Materials. IEEE: Piscataway, NJ, USA, 2004. [[CrossRef](#)]
30. Rezo, V.; Weis, M.; Micjan, M.; Nevrela, J.; Novota, M.; Szobolovsky, R. System for Measuring Small Currents. Utility Patent Number PUV 223-2024, 30 December 2023. (In Slovakia)
31. Rezo, V.; Weis, M.; Micjan, M.; Nevrela, J. Portable Biomarker Analysis Device and Its Mode of Operation. Utility Patent Number PUV 111-2024, 28 June 2024. (In Slovakia)
32. Rezo, V.; Weis, M.; Micjan, M.; Nevrela, J. Portable Biomarker Analysis Device and Its Mode of Operation. Design Number PD 52-2024, 28 June 2024. (In Slovakia)

**Disclaimer/Publisher’s Note:** The statements, opinions and data contained in all publications are solely those of the individual author(s) and contributor(s) and not of MDPI and/or the editor(s). MDPI and/or the editor(s) disclaim responsibility for any injury to people or property resulting from any ideas, methods, instructions or products referred to in the content.